catalysts

MDPI

Article

FeCrAlloy Monoliths Coated with Ni/Al_2O_3 Applied to the Low-Temperature Production of Ethylene

Paula Brussino [1], Juan Pablo Bortolozzi [1], Oihane Sanz [2], Mario Montes [2], María Alicia Ulla [1] and Ezequiel David Banús [1,*]

[1] Instituto de Investigaciones en Catálisis y Petroquímica, INCAPE (UNL-CONICET), Santiago del Estero 2829, 3000 Santa Fe, Argentina; pbrussino@fiq.unl.edu.ar (P.B.); jpbortolozzi@fiq.unl.edu.ar (J.P.B.); mulla@fiq.unl.edu.ar (M.A.U.)

[2] Departamento de Química Aplicada, Universidad del País Vasco (UPV/EHU), 20018 San Sebastián, Spain; oihane.sanz@ehu.eus (O.S.); mario.montes@ehu.es (M.M.)

* Correspondence: edbanus@fiq.unl.edu.ar; Tel.: +54-342-453-6861

Received: 24 May 2018; Accepted: 4 July 2018; Published: 19 July 2018

Abstract: This paper investigates the oxidative dehydrogenation of ethane to produce ethylene at low temperatures (500 °C) in metallic structured substrates. To check this point, the FeCrAlloy® monoliths with different channel sizes (289–2360 cpsi) were prepared. The monoliths were coated with a Ni/Al_2O_3 catalyst (by washcoating of alumina and the latter nickel impregnation) and characterized by Scanning Electron Microscopy and Energy-Dispersive X-ray analysis (SEM-EDX), Temperature-Programmed Reduction (TPR), X-ray Diffraction (XRD) and X-ray Photoelectron Spectroscopy (XPS). The catalytic results showed that all monoliths coated with ~300 mg of catalyst presented similar ethane conversion (15%) at 450 °C. However, the lowest selectivity to ethylene was found for the monolith with the lower channel size and the higher geometric surface area, where a heterogeneous catalyst layer with Ni enriched islands was generated. Therefore, it can be said that the selectivity to ethylene is linked to the distribution of Ni species on the support (alumina). Nevertheless, in all cases the selectivity was high (above 70%). On the other hand, the stability in reaction tests of one of the coated monoliths was done. This structured catalyst proved to be more stable under reaction conditions than the powder catalyst, with an initial slight drop in the first 8 h but after that, constant activity for the 152 h left.

Keywords: FeCrAlloy monoliths; Ni/Al_2O_3; oxidative dehydrogenation of ethane; ethylene

1. Introduction

Ethylene is one of the major building blocks in the petrochemical industries as it is mainly used for the synthesis of polyethylene and other compounds as acetaldehyde, ethanol, ethyl chloride, and ethylbenzene [1,2], which are important reactants for the synthesis of the everyday-life products. Between 2011 and 2016, ethylene world consumption grew at an average rate of about 3% per year, while its capacity increased at 2%, leading to higher utilization rates. Furthermore, this olefin consumption is expected to grow at about 3–4% per year over the next five years [3].

Currently the production of ethylene consumes many energetic resources because it is produced by the steam cracking of ethane or naphtha and the thermal cracking of petrochemical feedstocks such as naphtha, propane, and gas oil. Both processes operate at temperatures over 800 °C. These have important disadvantages as low olefin selectivity and raw material loss through coke formation, requiring shutdowns and maintenance [4,5].

The increase in the demand of ethylene requires cleaner and more efficient technologies, and the ethane oxidative dehydrogenation (ODE) looks like an interesting option (Scheme 1—green). This

reaction has many advantages: it is an exothermic reaction, operated at lower temperatures than the steam cracking (near to 500 °C), and it is more selective. In addition, it does not form carbon [4] and it is thermodynamically favored [6]. Therefore, this technology became interesting due the discovery of great reserves of shale gas in different parts of the world, given that in the shale gas the amount of ethane is significant [7,8].

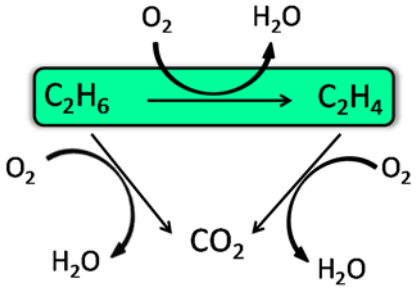

(**a**)

$$2\,C_2H_6 + O_2 \longrightarrow 2\,C_2H_4 + 2\,H_2O \quad \Delta H^0 = -105\ kJ/mol$$

$$2\,C_2H_6 + 7\,O_2 \longrightarrow 4\,CO_2 + 6\,H_2O \quad \Delta H^0 = -1428\ kJ/mol$$

$$C_2H_4 + 3\,O_2 \longrightarrow 2\,CO_2 + 2\,H_2O \quad \Delta H^0 = -1323\ kJ/mol$$

(**b**)

Scheme 1. (**a**) Ethane oxidative dehydrogenation (ODE) reaction triangle and (**b**) involved reactions.

For this reaction, an active and selective catalyst is necessary, since the total oxidation of ethane and ethylene also occur (Scheme 1). These two side reactions consume both the reagent and the product respectively, favoring the production of carbon dioxide and consequently diminishing the selectivity to ethylene. Numerous catalysts have been studied for the oxidative dehydrogenation of ethane (ODE) reaction [9,10], and some of the most investigated are the nickel-based catalysts. Nickel oxide is very active for ethane conversion, but its selectivity is poor. This parameter is key for an industrial application and it can be increased if the nickel oxide is dispersed in a high surface material as Al_2O_3 [11,12], TiO_2 [13], MgO [14], ZrO_2 [15], or clay [16]. Another route to improve the selectivity is to modify nickel oxide with high valence cations [17–19], but the deposition of these catalytic systems on a structured substrate is quite complex.

When a possible industrial application is considered, structured catalysts are good candidates. These systems have many advantages in comparison with the powder or pellet ones. Some of them offer lower pressure drop, higher energy efficiency, allow detailed designs, and ease scaling-up, among others [20,21]. The substrates that have been studied for the preparation of structured catalysts are ceramic foams [22], ceramic monoliths [23–25], ceramic papers [26–28], metallic foams [22,29], and metallic monoliths [5,30].

As the ODE reaction is exothermic, the use of a metallic substrate would be adequate due to their high thermal conductivity, which would result in a better temperature control [31,32]. Taking this into account, FeCrAlloy® monoliths would be suitable substrates because the thermal treatment generates a rough alumina layer which improves the catalyst particles anchorage on the metallic surface [32].

The objective of this work is to explore the use of FeCrAlloy® monoliths as structured substrates for catalytic devices used for the ODE reaction. For this purpose, the effect of the monoliths channel sizes on the Ni/Al_2O_3 catalyst deposition and the catalytic activity of each structured catalyst is studied. The technique that was used to deposit the catalytic coating was developed in a previous work [24]. Additionally, the catalytic results (activity, selectivity, and stability) of one of the structured catalysts have been compared with the corresponding powder catalyst.

2. Results

2.1. Preparation of the Structured Catalysts

A structured catalyst is composed of three parts: the substrate (FeCrAlloy® monolith in our case), the true catalytic support (alumina), which is the one that exposes the high specific surface area, and the active phase (Ni) that is dispersed over the surface of the support, the alumina. In our case, the

monoliths with different cell density, and therefore different geometric surfaces, were loaded with the same amount of alumina that will therefore expose the same surface area for Ni dispersion.

The FeCrAlloy® substrates used in this work are shown in Figure 1. These were named in order of ascending channel size as M1, M2, and M3. In addition, an M3 inserted in a cylindrical cartridge was prepared and it was denominated M3C.

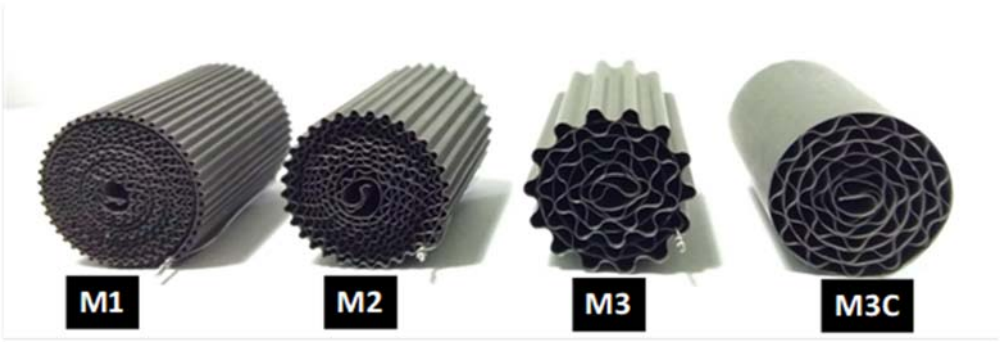

Figure 1. FeCrAlloy® monoliths used as substrates for the catalytic coatings depositions.

Table 1 shows a summary of preparation conditions, designations of the structured catalysts, and optical microscope photographs of the frontal and lateral sections for the alumina-washcoated monoliths. Centrifugation conditions refer to that used to eliminate the excess slurry after washcoating.

Table 1. Characteristics and preparation conditions of the coated substrates.

Coated Substrates	Frontal Section	Lateral Section	Centrifugation Conditions (Al_2O_3)	Al_2O_3 Coatings	Al_2O_3 Specific Load (mg/cm^2)
Al-M1	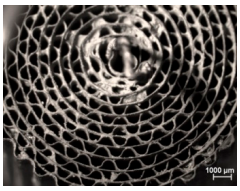	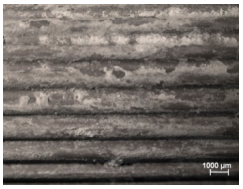	2000 rpm 5 min	2	0.56
Al-M2	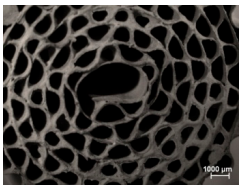	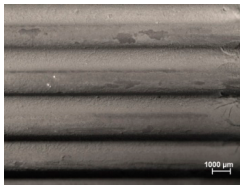	400 rpm 1 min	2	0.85
Al-M3	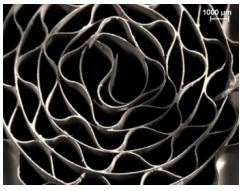	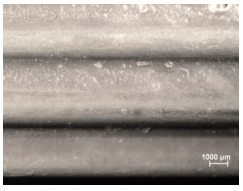	400 rpm 1 min	4	1.87
Al-M3C	-	-	400 rpm 1 min	5	1.68

Similar amounts of alumina were deposited (~300 mg/structured substrate) in all cases. Nevertheless, the number of coatings required to obtain the target catalyst loading decreased with the monoliths cell density. This is due to the higher geometric surface area of the former (see experimental part). However, for the Al-M1 monolith, with the highest cell density, and the M2 monolith, the same

number of coatings was needed. This is a consequence of the different centrifugation conditions used to coat M1, which were necessary to avoid the obstruction of the channels.

From the optical images of Table 1, it can be observed that the distribution of the alumina coating in Al-M1 was less homogeneous (lateral section), but the channels were not obstructed (frontal section). On the other hand, the Al-M2 and Al-M3 systems presented a homogeneously distributed alumina coating (lateral section) due to higher alumina layer thickness.

2.2. Structured Catalysts Characterization

An important aspect in a structured catalyst is the adherence between the catalytic film and the structured substrate. To study this adherence, the ultrasonic test was used. Figure 2 shows the results of the adherence test. It can be seen that catalyst adherence is very high in all the structured catalysts, higher than 90%. However, the anchoring of the catalyst coating to the structure was higher as the channel size diminished: Ni-Al-M1 > Ni-Al-M2 > Ni-Al-M3. Decreasing the channel size increases the geometric surface area, and thus the catalytic layer is thinner. In addition, as the hydraulic diameter decreases, the geometrical constraints increase [33]. Nevertheless, at the same channel size but comparing with and without the covering cartridge of the structured catalyst (Ni-Al-M3C and Ni-Al-M3), the adherence was higher in the first case. It is possible that the covering cartridge induces an extra protection, suggesting that in the other systems the major loss of catalytic coating comes from the external part.

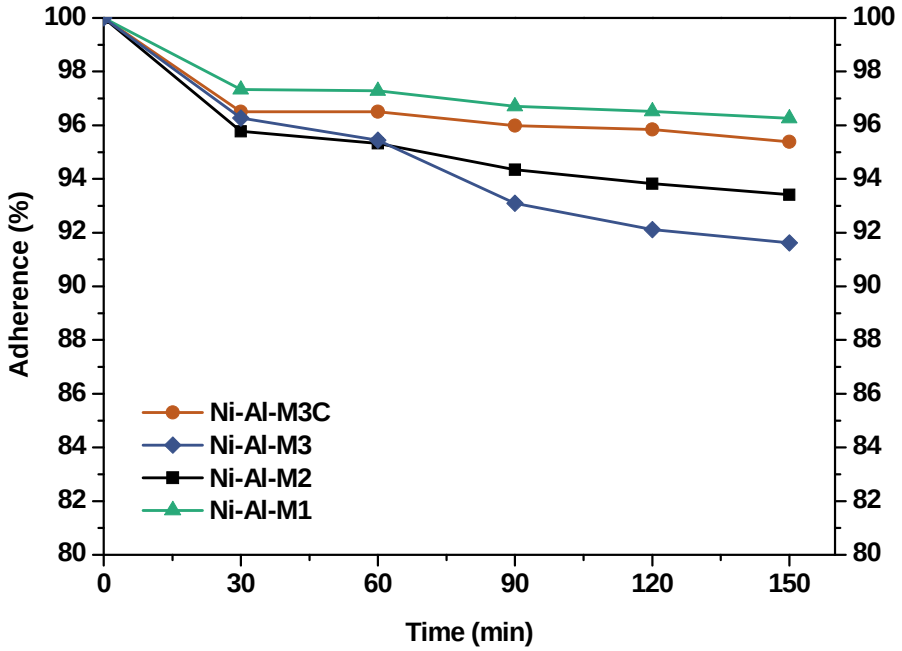

Figure 2. Adherence tests applied to the structured catalysts.

The morphology of the catalytic coatings and the elemental composition (semi quantitative) were analyzed by SEM-EDX (Tables 2 and 3). Three areas (100 × 100 μm) of a valley were used to obtain information about the composition along one channel of a monolith (Figure 3). The studied areas were called middle (M), intermediate (I), and end (E), which correspond to three relative longitudinal positions: M (l/L = 0.5), I (l/L = 0.25) and E (l/L = 0), as shown in Figure 3. The first and last refer to the middle and the end of the monolith in height, whereas the "I" stands for an intermediate area between these two. In each of these areas, three punctual analyses of 0.2 μm^2 (average value reported in Tables 2 and 3) were applied and they were marked in the micrographs with a lightening (red if the values highly exceeded the nominal Ni/Al ratio). The values of Ni/Al, Fe/Al and Cr/Al of the "dots"

are the average values of the three points that were analyzed. The catalytic systems were prepared with 25 wt. % Ni with respect to the alumina weight; hence the nominal Ni/Al molar ratio is around 0.2.

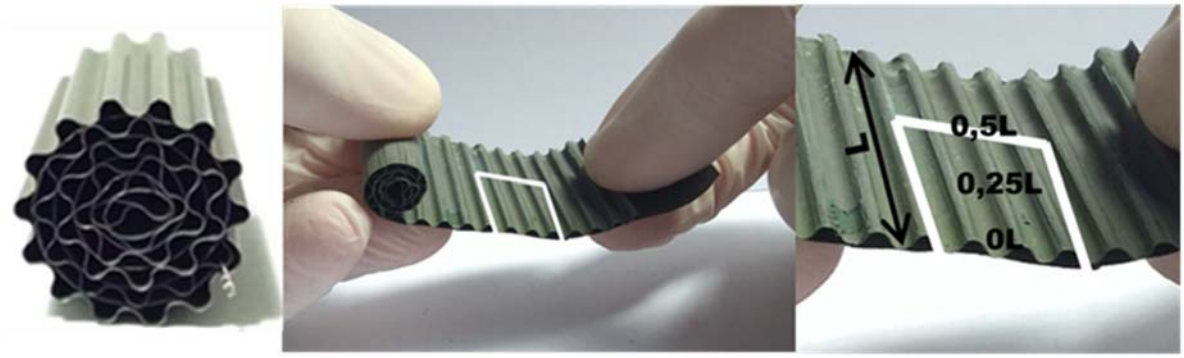

Figure 3. Illustration of the studied area of each monolith for SEM and EDX.

The results of Table 2 (Ni-Al-M3) show that there are small morphological differences. Also, some cracks are present in the intermediate area (near to the end of the monolith). The Ni/Al atomic ratios found in all the areas were slightly higher than the nominal one, around 0.27–0.32, but the higher values were found in the edge, where the analysis showed accumulations of active phase (red lightening points). It can be said that the Ni particles are well distributed, but some zones present some accumulations that may be due to the fact that they were dried vertically producing $Ni(NO_3)_2$ accumulations in the monoliths ends.

On the other hand, the Ni/Al ratios found in the middle and intermediate areas of Ni-Al-M3C (Table 2) resulted similar to those of Ni-Al-M3 (Table 2), whereas at the end area marked accumulations were spotted, exceeding the nominal value. When the alumina layer is deposited, during the drying stage it accumulates in the monoliths ends. Consequently, the intra and inter particles porosity is higher on those areas and the nickel solution gets trapped in them. In addition, the Fe/Al and Cr/Al ratios were also practically null in all the analyzed areas, indicating that the catalytic film would have a similar thickness than the Ni-Al-M3 coating.

The Ni-Al-M2 structured catalyst (Table 3) presented similar morphology and also the accumulation at the edge of the monolith. In the middle area, the coating presented more roughness compared to the other zones of analysis and the Ni/Al ratios resulted lower than those of Ni-Al-M3 and Ni-Al-M3C. Moving along the channel to the end of the monolith, the film got thicker and these marked accumulations were visualized. In the edge area the Ni/Al ratios were 0.76 and 1.07, whereas in the other ones they were around 0.14–0.17.

The Ni-Al-M1 system (Table 3) presented a very different morphology compared to all the other ones. The catalytic film is thinner, producing higher Fe/Al and Cr/Al ratios. This could be related to the centrifugation conditions, and the high geometric surface area. Particularly, in the middle area (M), the punctual analysis showed Fe/Al and Cr/Al ratios of 0.10 and 0.24, probably as a consequence of some heterogeneity in the FeCrAlloy®. In addition, a great amount of catalyst islands was observed in this coating. The EDX analysis in these sectors showed values of Ni/Al around 0.25–0.30, whereas in the flatter zones these values were lower (Ni/Al = 0.12–0.22). This is also related to the porosity of the support. When alumina gets accumulated its porosity is higher, allowing a greater amount of nickel solution to get trapped, increasing the Ni/Al ratio.

Table 2. SEM micrographs and elemental analysis of the Ni-Al-M3 and Ni-Al-M3C structured catalysts.

	SEM Image	Area			Dots		
		Ni/Al	Fe/Al	Cr/Al	Ni/Al	Fe/Al	Cr/Al
		Ni-Al-M3					
M	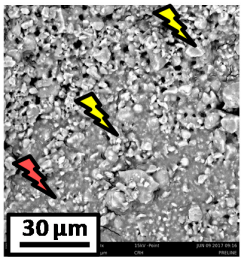	0.28	0.03	0.01	0.23	0.03	0.01
I	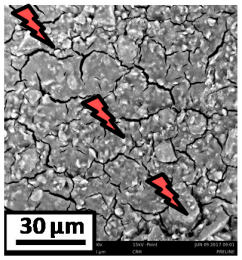	0.31	0.02	0.00	0.27	0.02	0.00
E	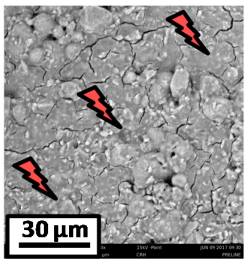	0.32	0.03	0.01	0.29	0.02	0.00
		Ni-Al-M3C					
M	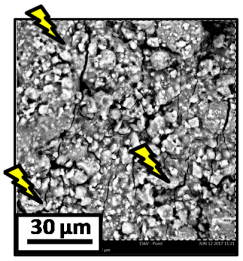	0.25	0.02	-	0.18	0.00	0.00
I	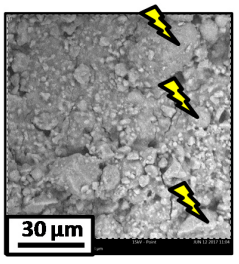	0.27	0.00	0.00	0.21	0.01	0.00
E	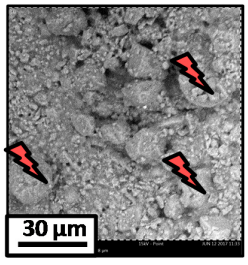	0.80	0.00	0.00	0.61	0.02	0.01

Table 3. SEM micrographs and elemental analysis of the Ni-Al-M2 and Ni-Al-M1 structured catalysts.

Optical Image	SEM Image	Area			Dots		
		Ni/Al	Fe/Al	Cr/Al	Ni/Al	Fe/Al	Cr/Al
		Ni-Al-M2					
M	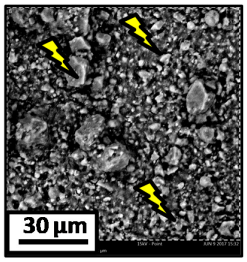	0.15	0.02	-	0.14	0.02	0.01
I	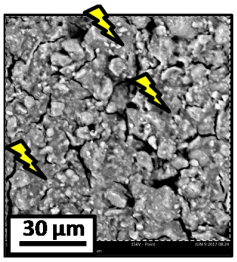	0.17	0.02	-	0.15	0.02	0.01
E	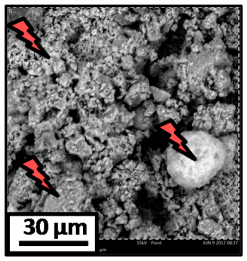	0.76	0.05	0.02	1.07	0.08	0.01
		Ni-Al-M1					
M	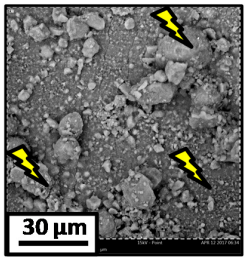	0.18	0.05	0.02	0.23	0.10	0.24
I	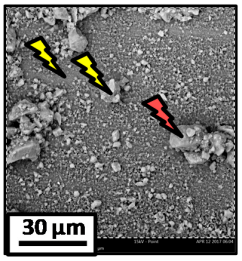	0.12	0.09	0.03	0.27	0.17	0.02
E	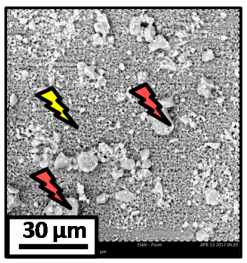	0.22	0.05	0.01	0.30	0.10	0.02

The distribution of Ni species on the alumina surface is a determining factor to obtain a homogeneous and well dispersed catalytic coating. Taking this into account, linear mappings of these coatings were obtained to study the element distribution in these catalytic films. Figure 4 shows these results for Ni-Al-M3 and Ni-Al-M1 in the intermediate area of the valley (Tables 2 and 3). The Ni active phase distribution along the Ni-Al-M3 catalytic system was more homogeneous than Ni-Al-M1 and its values were approximately constant and around 8.4% (atomic). The same behavior was observed for Al, where the relative constant value was 25.3%.

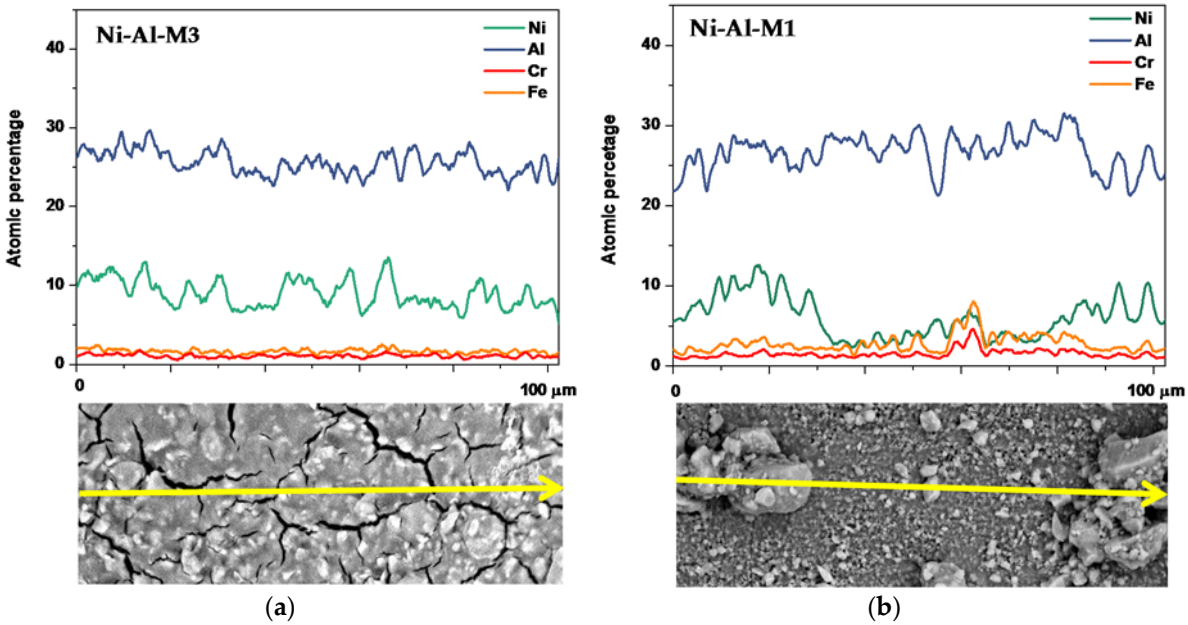

Figure 4. Linear mappings applied to (**a**) Ni-Al-M3 and (**b**) Ni-Al-M1 catalytic systems in the intermediate area of the valley.

However, in the case of the Ni-Al-M1 monolith nickel distribution was not homogeneous (Figure 4b). The linear mapping showed areas with catalyst agglomerations where the Ni/Al ratios were similar to those of Ni-Al-M3 (aluminum signal). Meanwhile, the flatter areas displayed lower Ni/Al ratios compared to those of Ni-Al-M3. The presence of these catalyst conglomerates could favor the nickel solution retention, during the impregnation.

With the aim of further studying the distribution of the different elements, mapping studies were carried out in the crests of monoliths channels, in which the contact between the smooth plate and the corrugated one takes place. The results for the Ni-Al-M1 structured catalyst is shown, since it was the same for all of the samples (Figure 5). The original SEM image shows areas where FeCrAlloy is visible and the other areas which are covered by the catalytic film (coating). The Ni mapping (green) registered these species mostly in the coating and even strongly in the visible catalyst islands, in agreement with the linear mappings. Opposite to this, Fe (yellow) was predominantly in the FeCrAlloy areas. Chromium on the other hand is well spread, in FeCrAlloy® areas as well as in the coating. This could be related to the fact that this element detection is poor and it is difficult to differentiate signal from noise.

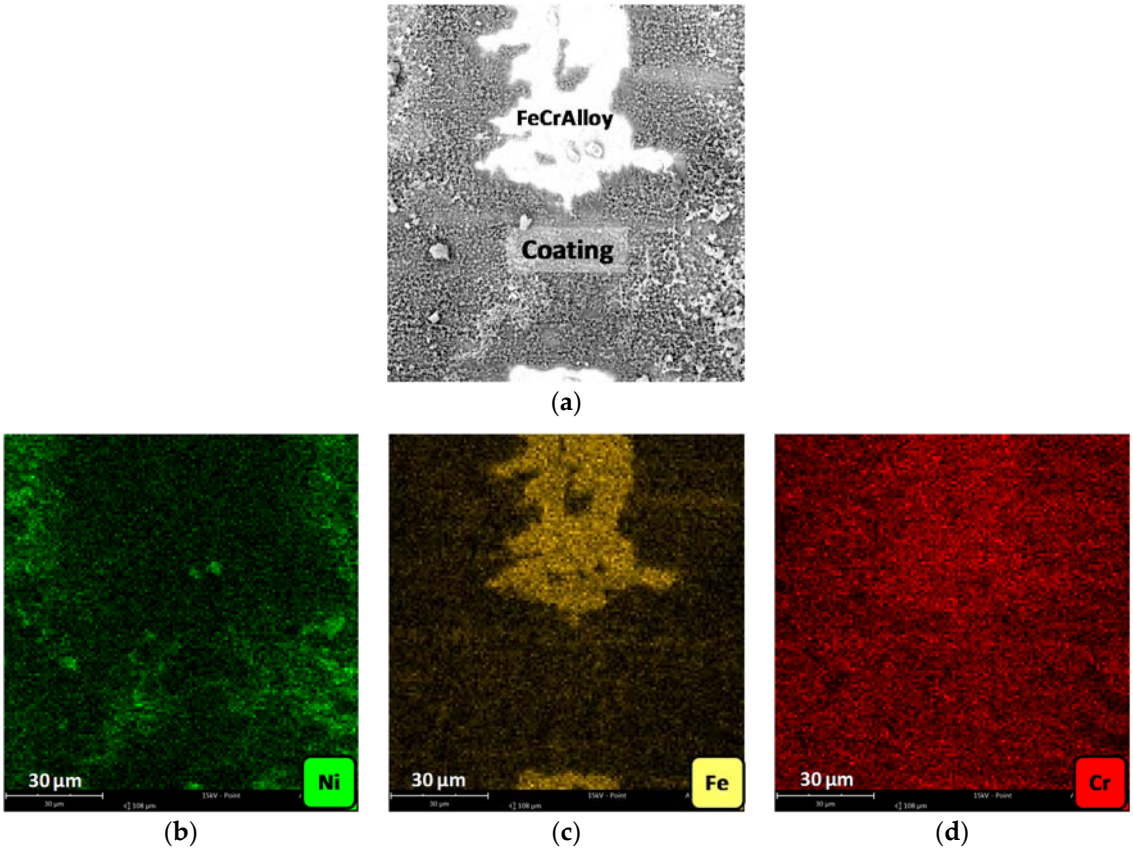

Figure 5. Mappings in an area of the Ni-Al-M1 structured catalyst: (**a**) SEM micrograph of the studied area, (**b**) Ni mapping, (**c**) Fe mapping and (**d**) Cr mapping.

To study the crystalline phases present in the catalysts, X-ray diffraction was used (not shown). The diffractograms corresponding to the un-treated metallic substrate (FeCrAlloy®), the calcined substrate (FeCrAlloy-900), γ-Al_2O_3 and the structured catalysts (Ni-Al-M1, Ni-Al-M2, Ni-Al-M3 and Ni-Al-M3C) were obtained. The FeCrAlloy® substrate presented two main diffraction lines which correspond to martensitic iron (Fe-Cr, JCPDS-ICDD 34–396). After the metallic monoliths were calcined at 900 °C for 22 h, a rough coating is formed due to the migration of Al_2O_3 from the FeCrAlloy® to the surface, so the diffraction lines that appeared in the FeCrAlloy-900 sample correspond to alumina. On the other hand, the catalytic systems showed the signals of γ-Al_2O_3 which corresponds to the alumina coating (JCPDS-ICDD 10–425), and a strong diffraction at 43° which could be associated with the Fe-Al system (JCPDS-ICDD 33-20). No diffractions corresponding to NiO were detected, probably due to small and well dispersed NiO particles over the alumina surface. For comparison, the XRD diffractogram was also obtained for the powder catalyst. The characteristic peaks of the support, Al_2O_3, were also observed with those of the NiO (JCPDS-ICDD 42-1467).

The structured catalyst surfaces were analyzed through XPS (Figure 6). It is known that bulk NiO presents a double Ni $2p_{3/2}$ main peak around 854 eV [34]. In this case, all Ni $2p_{3/2}$ principal peaks were symmetric. Moreover, the binding energies (BE) of Ni-Al-M2, Ni-Al-M3 and Ni-Al-M3C were quite similar (855.5–856 eV). Particularly the Ni-Al-M3 and Ni-Al-M3C structured catalysts presented practically the same BE values. These BE values are indicative of Ni^{2+} species highly interacting with the alumina used as support (γ-Al_2O_3) [11]. On the other hand, for the Ni-Al-M1 monolith the Ni $2p_{3/2}$ peak was better fitted with two components, both with a FWHM of ~3.3 eV and similar to those of the other structured catalysts. One of these components was 856.6 eV, indicating the presence of Ni^{2+} species highly interacting with alumina. The other signal was found at 854.8 eV and it corresponds to Ni^{2+} species with low interaction with alumina, similar to that of bulk NiO. This suggests that these

latter Ni^{2+} species are highly agglomerated and poorly interacting with the support. These results are in agreement with what was observed by SEM and EDX. The Ni-Al-M1 system showed a great amount of catalyst islands where the nickel solution got trapped and this nickel species (different from the ones in the flatter areas) have similar properties to those of bulk NiO, unlike the other structured catalysts.

The XPS spectrum of the powder catalyst was also obtained for comparison (Figure 6). In this case the Ni $2p_{3/2}$ peak presented the contribution of two Ni^{2+} species, one at 856.3 eV and the other at 854.6 eV. The former is associated to highly interacting nickel species whereas the latter one corresponds to weakly interacting nickel species.

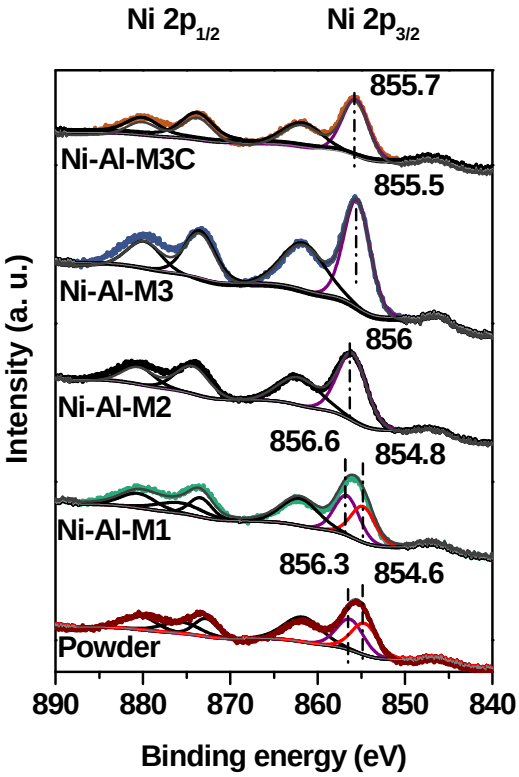

Figure 6. XPS spectra in the Ni 2p region of all the structured catalysts and the powder catalyst.

As these catalysts follow a redox mechanism, the analysis of their TPR profiles is of interest. Figure 7 shows the results for these structured catalytic systems and the one corresponding to pretreated FeCrAlloy® (FeCrAlloy-900). The profile corresponding to the pretreated metallic monolith was obtained to discard that any of the peaks of the structured catalysts belong to an oxide coming from the substrate.

In all the cases, the profiles extend from around 300 to 850 °C [35]. This denotes that there are several Ni species with different interaction with the alumina. There are peaks at low (300–400 °C), medium (400–650 °C) and high temperatures (650–800 °C). The first ones correspond to Ni species with weak interaction with alumina (bulk-like NiO) [36], whereas the ones at 400–650 °C are indicative of higher interactions with the support [37]. Finally, the peaks at 650–800 °C, present in all the catalytic systems, can be assigned to the reduction of highly dispersed non-stoichiometric amorphous nickel-aluminate spinels and bulk nickel-aluminates [38]. The Ni-Al-M1 catalyst presented a marked peak at 340 °C, evidencing the presence of some Ni^{2+} species poorly interacting with alumina, similar to that of bulk or free NiO [36,39,40]. As the temperature rises, more signals appear and they are indicative of nickel species with a higher interaction with the support. The maxima of the main peak of all of the catalysts are between 450–490 °C, suggesting that the majority of these have an intermediate interaction with the support. In addition, comparing Ni-Al-M1 and Ni-Al-M2, the temperature

maximum of Ni-Al-M1 (T_{max}) was slightly higher, which is consistent with the XPS results; the BE of the highly interacting species of Ni-Al-M1 (856.6 eV) was higher than the one of Ni-Al-M2 (856 eV). Furthermore, Ni-Al-M3 and Ni-Al-M3C presented quite similar maximum temperatures in their TPR profiles and similar BE in their XPS spectra (Figure 6). These results indicate that the properties of Ni-Al-M3 and Ni-Al-M3C are quite similar, both in the bulk as in the surface of the catalytic coatings.

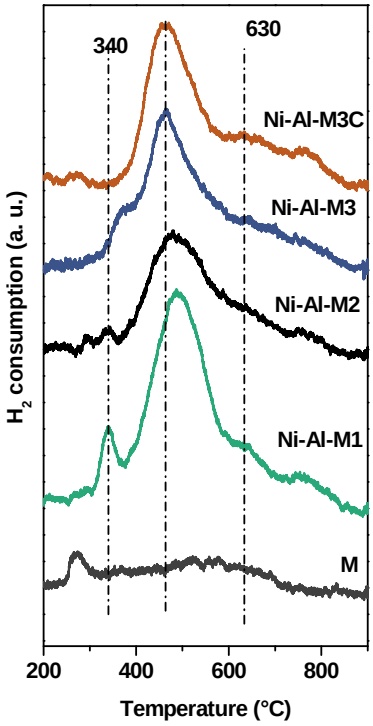

Figure 7. TPR profiles of the structured catalysts and a FeCrAlloy® sheet calcined at 900 °C for 22 h (M).

2.3. Catalytic Behavior in the ODE Reaction

As mentioned above, the first part of the catalytic tests is the analysis of the ethane conversion with the temperature. It was performed by varying the reaction temperature from 300 to 450 °C at a fixed W/F ratio of 0.48 g·s/cm^3 (Figure 8a).

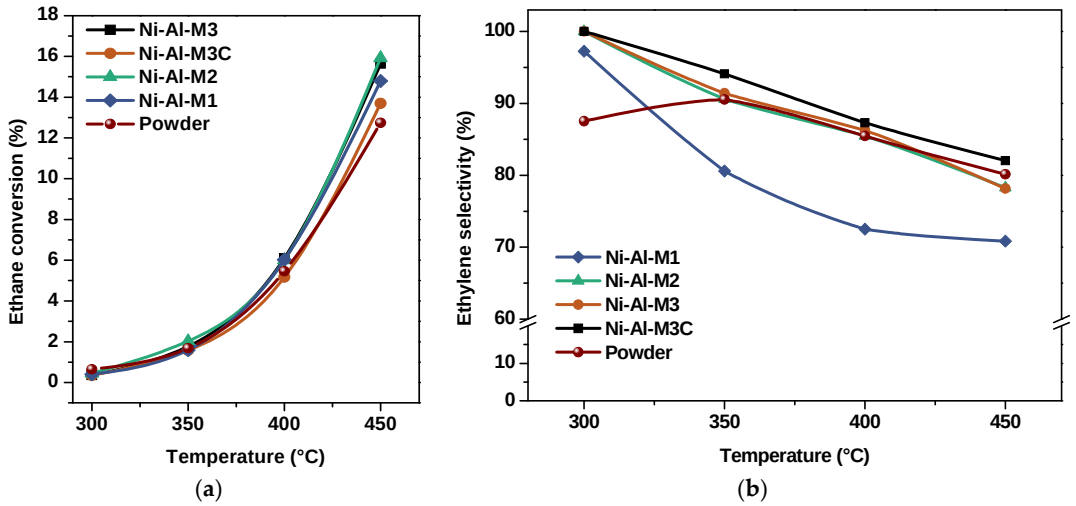

Figure 8. Catalytic activity at W/F = 0.48 g·s/cm^3. (**a**) Ethane conversion and (**b**) ethylene selectivity.

Table 4 shows these results at 450 °C. Ethylene selectivity behavior with the temperature is shown in Figure 8b.

Table 4. Catalytic data at W/F = 0.48 g·s/cm^3 and 450 °C (6% C_2H_6, 6% O_2 and He balance).

Catalyst	Ethane Conversion (%)	Ethylene Selectivity (%)
Ni-Al-M1	14.8	70.8
Ni-Al-M2	15.9	78.3
Ni-Al-M3	15.7	78.2
Ni-Al-M3C	13.7	82.1
Powder	12.7	80.1

Ethane conversion was similar for all the structured catalysts, indicating that the channel size did not influence this parameter. However, the Ni-Al-M3C system presented the lowest conversion value. This could be related to their slightly different Ni loadings (Table 2). For the powder catalyst, the ethane conversion was slightly lower compared to the structured catalysts but still similar. On the other hand, the selectivities were similar for Ni-Al-M2, Ni-Al-M3 and Ni-Al-M3C, whereas for Ni-Al-M1 the selectivity to ethylene was lower. Meanwhile, the selectivity of the powder system was in line with the values found for Ni-Al-M2, Ni-Al-M3 and Ni-Al-M3C.

The homogeneous distribution of the support (alumina) onto the monoliths is a significant factor to take into account in Ni/Al_2O_3 catalysts applied to the ODE reaction. In order to obtain high selectivity to the olefin, Ni^{2+} species need to be well dispersed on the support [24]. Taking this into account, the second part of the catalytic tests is important because it relates the selectivity to the olefin with the alkane conversion (varied with different W/F) at a fixed temperature (Figure 9). Therefore, it shows the selectivity behavior of the structured catalysts. As mentioned above, the reaction pathway follows a triangle between ethane, ethylene, and carbon dioxide. The points in Figure 9 for each catalytic system can be linearly fitted, where the slopes and intercepts relate with the ethylene selectivity. It is well known that in the oxydehydrogenation reaction of ethane, the selectivity of the direct oxidation of ethane to CO_2 can be related to the difference to 100 from the selectivity to ethene at zero conversion, and the selectivity of the oxidation of ethene to CO_2 with the slope of the selectivity to ethene vs. conversion [11,41]. In fact, at zero conversion there is only ethane that can be converted to CO_2, and as the conversion increases, the loss of selectivity to ethene (negative slope) must be related to the partial transformation of this ethene into CO_2.

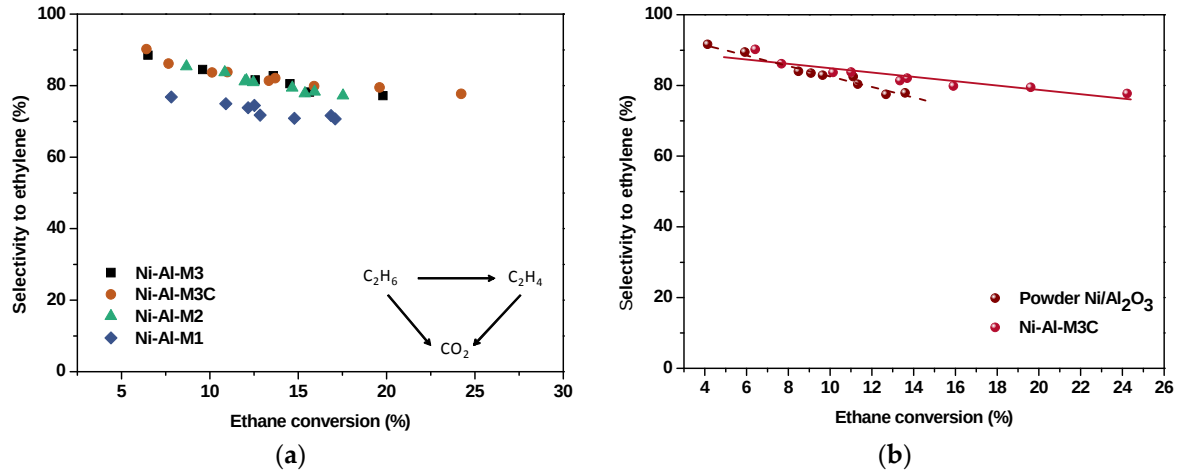

Figure 9. Ethylene selectivity vs. ethane conversion at 450 °C—Variable W/F (0.15–1.3 g·s/cm^3), (**a**) structured catalysts and (**b**) comparison between Ni-Al-M3C and the powder catalyst.

From the analysis of Figure 9a, it can be noticed that the selectivity tendencies of almost all the structured catalysts are similar, having similar degree of ethylene oxidation. This could be related to the fact that all the structured catalysts have the same catalytic formulation and the same catalyst loading. In addition, it appears that at relatively high conversion values, the selectivity maintains a flat trend with the conversion level. Nevertheless, Ni-Al-M1 catalytic system presented lower selectivity to the olefin compared to the other ones. While Ni-Al-M2, Ni-Al-M3 and Ni-Al-M3C presented high selectivity (around 80–90%), Ni-Al-M1 showed values around 70–80%. Another aspect to observe from Table 4 and Figure 8 is that there are no significant differences in the catalytic behavior of Ni-Al-M3 and Ni-Al-M3C, indicating that covering the outside of the original metallic monolith does not induce significant changes.

Despite the similar selectivity values found for the structured and powder catalysts, the selectivity behavior with the conversion was also studied for the powder formulation. This was carried out with the aim to compare the response of both systems. These results are displayed in Figure 9b. In spite of the highly elevated ethylene selectivities at low conversion values in both catalytic systems, there was a marked drop for the powder catalyst compared to the structured catalyst. This indicates that there is a higher tendency to oxidize the produced ethylene in the powder formulation.

Study of Stability in Reaction

A study of stability in reaction was performed for the Ni-Al-M3C system, considering its selectivity and its adherence, and it was compared with the corresponding powder catalytic formulation. This was performed to analyze if the structured catalyst was effectively more efficient than the powder catalyst. The ethane conversion and the ethylene selectivity were monitored at 450 °C over a period of time of 160 h maintaining the W/F at 0.48 g·s/cm^3 (Figure 10).

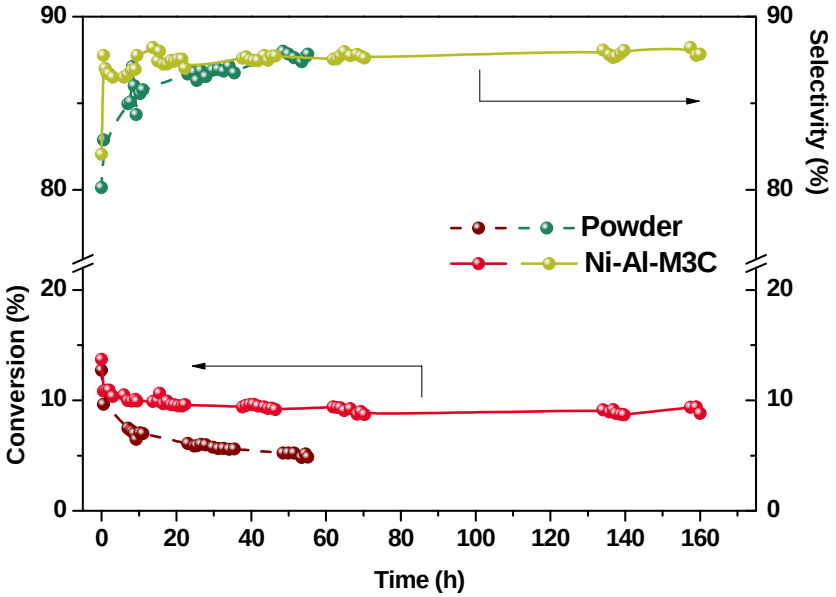

Figure 10. Structured and powder catalysts stability in reaction, T = 450 °C and W/F = 0.48 g·s/cm^3.

In both systems the conversion suffered a drop during the first minutes of reaction. Nevertheless, the drop in the activity of the powder catalyst was higher than that of the structured one. After 8 h under reaction, the structured catalyst lost 27% of its initial activity, while this value for the powder was of 45%. Furthermore, after this time the conversion remained constant for the structured catalyst for the remaining 152 h. On the other hand, the ethylene selectivity increased due to the conversion drop in both systems, maintaining the structured catalyst a very high value (~88%).

3. Discussion

3.1. Mechanical Stability of the Catalytic Coatings

The adherence results (Figure 2) were in line with what was demonstrated by L.C. Almeida et al. [33]. The size of the channel affects the anchoring of the catalytic film to the substrate's surface. This is related with the hydraulic diameter: the smaller this parameter, the higher the adherence and this is a consequence of geometrical constraints which increase as the channel size decreases. Furthermore, it seems that adding an external housing (M3C) induces an extra protection to the structure, improving the mechanical stability.

3.2. Nickel Species Distribution and Its Impact on the Catalytic Behavior

The performed characterization showed that the systems with bigger channel size (Ni-Al-M2, Ni-Al-M3, and Ni-Al-M3C) have a more homogeneous distribution of nickel species over the alumina surface, as remarked by the obtained linear mappings (Figure 4, Ni-Al-M3 representing the other systems) and the SEM micrographs. This is a consequence of the smaller geometric area exposed by these substrates which requires a thick coating film for the same total load (alumina loading ratio—Table 1), favoring the coating homogeneity. On the other hand, the Ni-Al-M1 sample presented several catalyst islands which held nickel species with similar properties to those of bulk NiO (Figure 4—Ni-Al-M1, Table 3), as a result of the high geometric area. This was also observed through the other characterization techniques. The TPR profiles (Figure 7) of the first three systems did not show the presence of weakly interacted Ni species, while in the case of the Ni-Al-M1 structured catalyst, a small peak at 340 °C appeared, indicating that there is a small amount of nickel species with poor interaction with alumina, in agreement with SEM and EDX. Moreover, Ni-Al-M1 and Ni-Al-M2 presented Ni species with higher interaction with the support than those of Ni-Al-M3 and Ni-Al-M3C (higher T_{max}), but Ni-Al-M1 analysis showed the presence of weakly interacted nickel species (340 °C). Furthermore, the surface analysis was consistent with TPR, as it revealed that the Ni^{2+} species of Ni-Al-M3 and Ni-Al-M3C are highly interacting with the support. The Ni $2p_{3/2}$ BE were about 855.5 eV and the BE found in Ni-Al-M2 was a little bit higher, 856 eV. This was also the case for the Ni-Al-M1 system. The Ni-Al-M1 catalyst presented a contribution of nickel species with higher interaction with alumina (856.6 eV), which is in line with the higher T_{max} revealed by TPR, and some Ni species with weak interaction with alumina, with a BE value near that of volumetric NiO (Figure 5), as spotted by TPR (340 °C). All of these results are in line with what was seen by SEM and EDX.

In terms of catalytic performance, at a constant W/F ratio the ethane conversion was very similar in all cases (Table 4) indicating that all the structured catalysts have a similar number and nature of active sites. This is consistent because all of them were prepared with the same amount of nickel, indicating that the preparation method is adequate. Moreover, the EDX analysis (by area and punctual) showed that all the catalytic systems have a Ni/Al ratio of around 0.20, excluding some areas and points where the ratio was higher. Specifically, for the Ni-Al-M2 and Ni-Al-M3C samples these higher ratios were a consequence of the nickel solution accumulation at the end of the monolith during the drying stage.

Olefin selectivity was the most affected catalytic parameter by the distribution of nickel species. At a constant temperature, the selectivity to ethylene was lower for the Ni-Al-M1 structured catalyst compared with the other systems (Figure 8a). It is known in the literature that free NiO is active for the ODE reaction but highly unselective [41,42]. Through TPR, XPS, and SEM-EDX nickel agglomerates were detected, which are not bulk NiO but they contain Ni species with very poor interaction with alumina. This explains the lower selectivity in this system. Still, this structured catalyst presented very high selectivity to ethylene, because the rest of the Ni species have strong interaction with alumina, as revealed by TPR and XPS. On the other hand, the elevated selectivity of Ni-Al-M2, Ni-Al-M3 and Ni-Al-M3C is generated by the homogeneous distribution of Ni particles and their high interaction with the support.

Comparing the two structured catalysts with the same channel size (Ni-Al-M3 and Ni-Al-M3C), it becomes clear that adding a covering housing to the Ni-Al-M3 system does not change the active sites, since the physicochemical characterization was practically the same for both of them (TPR profiles and XPS spectra). The only difference observed between these two was the ethane conversion values (Figure 8 and Table 4), which were a bit higher for the Ni-Al-M3 structured catalyst probably due to its slightly higher Ni/Al ratios (EDX).

Finally, it has been observed that the structured catalyst was more stable under the reaction stream than the powder catalyst (Figure 10) probably due to its ability to remove the reaction heat, avoiding the generation of hot spots, that could produce catalyst sintering. Packed beds are characterized by few contact points between particles, resulting in insignificant heat transfer by thermal conduction. However, it is known that the heat transfer capacity can be increased by employing monolithic reactors prepared with metallic substrates [43]. In addition, the XRD technique showed the presence of NiO crystals, which would be bigger than the ones present in the structured catalysts and not well dispersed, since in these last no NiO diffractions were observed. This is in agreement with the XPS analysis, which displayed the presence of some poorly interacting Ni species (854.6 eV). Clearly, the monolithic catalyst prepared in this work showed promising stability, with high conversion and selectivity throughout the entire 160 h testing.

4. Materials and Methods

4.1. Preparation of the Structured Catalysts

The structured catalyst preparation was carried out in two steps. First, an alumina layer to be used as support for the active phase dispersion was deposited onto these monoliths channels. And then, nickel was dispersed by impregnation. For comparison, all the catalytic coatings were generated with quite similar mass (~400 mg). For the M3C system, previous to any deposition or immersion, this monolith was wrapped on the external sheet with Teflon® tape and then with heat-shrinkable rubber to avoid the generation of the catalytic coating over this sheet and ensure the suspension or solution flow only through the channels.

4.1.1. Substrates Pre-treatment

FeCrAlloy® (Goodfellow) monoliths fabricated with parallel and corrugated sheets were used as substrates (Figure 1) for the deposition of a Ni/Al_2O_3 coating. Further details are given in Table 5. These monolithic substrates were designated in order of ascending channel size as M1, M2, and M3. In addition to these monoliths, M3C structured substrate was prepared introducing the M3 monolith in a cylindrical cartridge or housing of FeCrAlloy® (50 μm).

Table 5. Properties of the FeCrAlloy® monoliths.

Monoliths Properties	M1	M2	M3	M3C
Cell density (cpsi)	2360	1330	289	289
Hydraulic diameter (μm)	361	475	1065	1065
Diameter (mm)	16	16	16	16
Length (mm)	30	30	30	30
Geometric surface area (cm^2)	521	420	207	222

These materials are not adequate as catalysts structured substrates by themselves due to their smooth surface. In order to obtain a rough surface and consequently to improve the anchorage of the catalytic coating, these monoliths were submitted to a heat treatment in a muffle in air at 900 °C for 22 h [32]. During the calcination process, an Al_2O_3 layer is formed with excellent roughness properties for the anchoring of the catalytic coating [44].

4.1.2. Al_2O_3 Layer Deposition

The washcoating method was selected to obtain the alumina layer. This technique consists of applying cycles of immersion in a suspension–elimination of suspension excess–drying–calcination until the final load is achieved [44].

The alumina suspension was prepared using the following components: H_2O, PVA (polyvinyl alcohol), colloidal Al_2O_3 (NYACOL® AL20DW, Ashland, MA, USA), powder Al_2O_3 Puralox® SBa230 (Sandton, South Africa) (milled), in the designated molar ratio, 3.15:0.09:1.12:1. Firstly, the Al_2O_3 Puralox® SBa230, (original particle size D_{50} = 45 μm) was ball milled at 169 rpm for 210 min to reduce the particle size to D_{50} = 21 μm. Then, the distilled water was heated under agitation at 80 °C and the PVA was dissolved. Next, the solution was cooled to 50 °C and the colloidal alumina (®) (Ashland, MA, USA) was incorporated dropwise. Finally, the ball-milled alumina powder was added slowly and the final slurry was left under agitation overnight. The pH was maintained at 4, a value away from the IEP of alumina, in order to favour the particles' repulsion and consequently improve the stability of the slurry.

The pretreated monoliths were immersed into the prepared suspension for 1 min and removed at constant speed (3 cm/min). Then, the excess of suspension was eliminated by centrifugation where different revolutions per minute and times were applied depending on the channel size. For the M3C, M3, and M2 systems the conditions were 400 rpm for 1 min, while for the M1 systems (presenting smaller channel size) they were 2000 rpm for 5 min. These values were selected to ensure that the channels were not plugged. After that, the alumina-coated monoliths were vertically dried in a stove for 1 h and, finally, they were calcined in a muffle at 550 °C for 2 h. The complete procedure describes a cycle, and it was repeated until the achieved alumina loading was approximately 300 mg per monolith. These alumina-coated monoliths were named as follows: Al-M1, Al-M2, Al-M3, and Al-M3C.

4.1.3. Incorporation of Nickel

To incorporate the active phase to the alumina-coated monoliths the impregnation method was used. In this case, the alumina coated monoliths were immersed in a 0.43 M nickel nitrate hexahydrate solution (Sigma-Aldrich®) for 1 min. Then, the excess of the solution was eliminated by centrifugation (400 rpm, 15 s for Al-M3C, Al-M3 and Al-M2; 2000 rpm, 1 min for Al-M1) and they were dried in a stove for 1 h. Samples were calcined in a muffle at 550 °C for 2 h. The final catalytic systems had ~25 wt. % Ni with respect to the alumina coating (which corresponds to ~18.75% Ni with respect to the catalytic coating amount, active phase plus support). The nickel weight percentage was calculated by weight difference, with the following equation:

$$wt.\%\ Ni = \frac{mg\ Ni}{mg\ Al_2O_3} \times 100\% \quad (1)$$

The final catalytic systems were denominated as: Ni-Al-M1, Ni-Al-M2, Ni-Al-M3, and Ni-Al-M3C.

4.2. Preparation of the Powder Catalyst

For comparison, the corresponding powder catalyst was prepared by wet impregnation, using a nickel concentration such that the final powder contained 25 wt. % Ni (with respect to the alumina weight). The alumina used as support was previously calcined at 500 °C for 4 h. After impregnation the solid was dried at 130 °C overnight and calcined at the same conditions as the structured catalysts.

4.3. Structured Catalysts Characterization

Optic microscopy: To analyze the general distribution of the catalytic coating and the presence of blocked channels a Leica S8 APO stereomicroscope (Leica AG, Wetzlar, Germany) was used.

Adherence tests: A Testlab TB04 equipment (40 kHz and 160 W) (Testlab SRL, Buenos Aires, Argentina) was used to study the coating weight loss caused when the structured catalysts were

exposed to an ultrasound bath. The monoliths were immersed into acetone and they were submitted to ultrasound at 25 °C for 30 min. Five consecutive tests were performed. The adherence is expressed as the percentage of the original coating weight remaining after the adherence test.

Scanning Electron Microscopy (SEM) coupled with Energy-Dispersive X-ray Analysis (EDX): A SEM Phenom World ProX instrument (Phenom World, Eindhoven, The Netherlands), operating at 15 kV of acceleration voltage, was employed. The elemental chemical analysis was performed using an EDX system coupled to this equipment. The results were obtained by the theoretical quantitative method (SEMIQ), which does not require standards. Linear mappings were taken along the coating. Pieces of the inner channels of the monoliths were analyzed.

X-ray Diffraction (XRD): X-ray diffractograms were obtained with a Shimadzu XD-D1 instrument (Shimadzu, Kyoto, Japan) with monochromator using Cu Kα radiation at a scan rate of 2°/min, from 2θ = 20 to 80°. The monoliths were put in a special sample holder for the XRD analysis.

Temperature Programmed Reduction (TPR): The profiles were obtained with a Micromeritics AutoChem II instrument (Micromeritics Instrument Corporation, Norcross, GA, USA) using a mixture of H_2/Ar (5%) as a reducing gas. The heating rate was 10 °C/min from room temperature to 900 °C. Pieces of the inner channels of the monoliths were cut and rolled up to fit the U-shaped reactor. These samples were pretreated in an oxygen atmosphere at 350 °C for 10 min.

X-ray Photoelectron Spectroscopy (XPS): Measurements were performed in a SPECS equipment (SPECS GmbH, Berlin, Germany) with a hemispherical PHOIBOS150 analyzer operating in the FAT mode. The spectra were obtained with a pass energy of 30 eV and Mg-Kα X-ray source power of 200 W. Samples were evacuated for 2 h in an ultra-high vacuum. The peak fitting was performed with the CASAXPS software and C 1s at 284.6 eV was used as reference. The monoliths were cut in pieces (inner channels) for their analysis.

4.4. Catalytic Behavior in the ODE Reaction

A flow system coupled to a gas chromatograph (Shimadzu® GC 2014, packed column: Hayesep D®) was used. The feed composition was 6% C_2H_6, 6% O_2 and helium as balance gas. The structured catalysts located in a quartz reactor (Ø = 16.3 mm). The thermocouple was placed as illustrated in [28]. Particularly, the Ni-Al-M3C structured catalyst was previously wrapped with quartz wool to force the feed flow through the channels, taking into account that the outer face of the housing was not coated with catalyst. The catalysts weight (alumina + active phase) was around 400 mg for each sample. Before the catalytic tests, each structured catalyst was calcined in air flow at 550 °C for 4 h. In the first part of the experiments, a fixed W/F ratio of 0.48 g·s/cm^3 was used and the temperature was varied between 300−450 °C. A second part of the tests was carried out setting a constant temperature of 450 °C and varying the W/F ratio (0.15–1.3 g·s/cm^3) in order to analyze the behavior of the selectivity with the conversion level. Closure of the carbon mass balance was 100 ± 2%. Carbon monoxide was not detected in the products stream after reaction. Quantification of ethane conversion ($X_{C_2H_6}$) and ethylene selectivity ($S_{C_2H_4}$) were based on the carbon mass balance and calculated as follows:

$$X_{C_2H_6}(\%) = \frac{[CO_2] + 2[C_2H_4]}{2[C_2H_6]} \times 100\% \quad (2)$$

$$S_{C_2H_4}(\%) = \frac{2[C_2H_4]}{[CO_2] + 2[C_2H_4]} \times 100\% \quad (3)$$

Stability tests were carried out at 450 °C and a fixed catalyst weight to total flow ratio of 0.48 g·s/cm^3. Ethane conversion and ethylene selectivity were monitored for a total time of 160 h for the structured catalyst and around 50 h for the powder formulation.

5. Conclusions

FeCrAlloy® monoliths are suitable substrates to deposit Ni/Al_2O_3 catalytic films, with excellent adherence (over 90% after 150 min of ultrasound). Furthermore, these structured catalysts are active and stable on the oxydehydrogenation of ethane at relative low temperatures. Depending on the channel size different preparation conditions were needed in order to obtain structured catalysts with all the channels unblocked. This was particularly the case of the catalytic system with the smaller channel size (Ni-Al-M1). Therefore, the obtained catalytic coating results were heterogeneous with a marked amount of catalyst islands. These accumulations have comparable properties to those of free NiO, which influence the catalytic performance, decreasing its selectivity to the desired product. Still, all the catalysts showed excellent values of ethylene selectivity, a parameter that is key for their practical application. These elevated selectivity values are reflected in the Ni^{2+} species, which have a strong interaction with the support as observed by TPR and XPS. In addition, the similar results found by these two techniques infer that the physicochemical properties remain along the catalytic coatings.

Moreover, the structured catalyst proved to be more stable under the reaction conditions than the powder catalyst, with a lower drop in its initial activity and with constant values of conversion and selectivity.

On the other hand, no marked differences were observed for the Ni-Al-M3 and the Ni-Al-M3C structured catalysts, neither in the characterization nor in the catalytic performance. Hence, taking into account the elevated adherence obtained with the Ni-Al-M3C system (>96%), this would be the selected structured catalyst to continue on studying with the purpose of improving the ethane conversion but maintaining its elevated olefin selectivity.

Author Contributions: P.B. prepared the structured catalysts, evaluated them in the reaction and participated in the writing and discussion of this paper; J.P.B., O.S., M.M. and M.A.U. participated in the redaction and discussion of the manuscript. E.D.B. constructed the metallic monoliths and supervised the work advising about the discussion and the conclusion sections.

Acknowledgments: The authors acknowledge the financial support received from ANPCyT, CONICET and UNL. Also, thanks are given to the Basque Government (IT1069-16) and the Spanish MINECO/FEDER (ENE2015-66975-C3-3-R and CTQ2015-73901-JIN) for the financial support.

Conflicts of Interest: The authors declare no conflict of interest.

References

1. World Ethylene World Analysis | IHS Markit. Available online: https://www.ihs.com/products/world-petro-chemical-analysis-ethylene.html (accessed on 15 September 2017).
2. Armstrong, R.; Hutchings, G.; Taylor, S. An Overview of Recent Advances of the Catalytic Selective Oxidation of Ethane to Oxygenates. *Catalysts* **2016**, *6*, 71. [CrossRef]
3. Ethylene-Chemical Economics Handbook (CEH) | IHS Markit. Available online: https://www.ihs.com/products/ethylene-chemical-economics-handbook.html (accessed on 7 October 2017).
4. Zhu, H.; Rosenfeld, D.C.; Harb, M.; Anjum, D.H.; Hedhili, M.N.; Ould-Chikh, S.; Basset, J.M. Ni-M-O (M = Sn, Ti, W) Catalysts Prepared by a Dry Mixing Method for Oxidative Dehydrogenation of Ethane. *ACS Catal.* **2016**, *6*, 2852–2866. [CrossRef]
5. Santander, J.A.; Boldrini, D.E.; Pedernera, M.N.; Tonetto, G.M. NiNbO catalyst deposited on anodized aluminum monoliths for the oxidative dehydrogenation of ethane. *Can. J. Chem. Eng.* **2017**, *95*, 1554–1561. [CrossRef]
6. Fung, V.; Tao, F.F.; Jiang, D. Understanding oxidative dehydrogenation of ethane on Co_3O_4 nanorods from density functional theory. *Catal. Sci. Technol.* **2016**, *127*, 113–131. [CrossRef]
7. Gaffney, A.M.; Mason, O.M. Ethylene production via Oxidative Dehydrogenation of Ethane using M1 catalyst. *Catal. Today* **2017**, *285*, 159–165. [CrossRef]
8. Baroi, C.; Gaffney, A.M.; Fushimi, R. Process economics and safety considerations for the oxidative dehydrogenation of ethane using the M1 catalyst. *Catal. Today* **2017**. [CrossRef]

9. Bañares, M.A. Supported metal oxide and other catalysts for ethane conversion: A review. *Catal. Today* **1999**, *51*, 319–348. [CrossRef]
10. Gärtner, C.A.; van Veen, A.C.; Lercher, J.A. Oxidative dehydrogenation of ethane: Common principles and mechanistic aspects. *ChemCatChem* **2013**, *5*, 3196–3217. [CrossRef]
11. Heracleous, E.; Lee, A.F.; Wilson, K.; Lemonidou, A.A. Investigation of Ni-based alumina-supported catalysts for the oxidative dehydrogenation of ethane to ethylene: Structural characterization and reactivity studies. *J. Catal.* **2005**, *231*, 159–171. [CrossRef]
12. Zhang, X.; Liu, J.; Jing, Y.; Xie, Y. Support effects on the catalytic behavior of NiO/Al_2O_3 for oxidative dehydrogenation of ethane to ethylene. *Appl. Catal. A Gen.* **2003**, *240*, 143–150. [CrossRef]
13. Sanchis, R.; Delgado, D.; Agouram, S.; Soriano, M.D.; Vázquez, M.I.; Rodríguez-Castellón, E.; Solsona, B.; Nieto, J.M.L. NiO diluted in high surface area TiO_2 as an efficient catalyst for the oxidative dehydrogenation of ethane. *Appl. Catal. A Gen.* **2017**, *536*, 18–26. [CrossRef]
14. Nakamura, K.-I.; Miyake, T.; Konishi, T.; Suzuki, T. Oxidative dehydrogenation of ethane to ethylene over NiO loaded on high surface area MgO. *J. Mol. Catal. A Chem.* **2006**, *260*, 144–151. [CrossRef]
15. Sakitani, K.; Nakamura, K.; Ikenaga, N.; Miyake, T.; Suzuki, T. Oxidative Dehydrogenation of Ethane over NiO-loaded High Surface Area ZrO_2 Catalysts. *J. Jpn. Petrol. Inst.* **2010**, *53*, 327–335. [CrossRef]
16. Solsona, B.; Concepción, P.; Lopez Nieto, J.M.; Dejoz, A.M.; Cecilia, J.A.; Agouram, S.; Soriano Rodriguez, D.; Torres, V.; Jiménez-Jiménez, J.; Rodriguez-Castellón, E. Nickel oxide supported on Porous Clay Heterostructures as selective catalysts for the oxidative dehydrogenation of ethane. *Catal. Sci. Technol.* **2015**, *6*, 3419–3429. [CrossRef]
17. Heracleous, E.; Lemonidou, A.A. Ni-Me-O mixed metal oxides for the effective oxidative dehydrogenation of ethane to ethylene—Effect of promoting metal Me. *J. Catal.* **2010**, *270*, 67–75. [CrossRef]
18. Zhu, H.; Dong, H.; Laveille, P.; Saih, Y.; Caps, V.; Basset, J.M. Metal oxides modified NiO catalysts for oxidative dehydrogenation of ethane to ethylene. *Catal. Today* **2014**, *228*, 58–64. [CrossRef]
19. Nieto, J.M.L.; Solsona, B.; Grasselli, R.K.; Concepción, P. Promoted NiO catalysts for the oxidative dehydrogenation of ethane. *Top. Catal.* **2014**, *57*, 1248–1255. [CrossRef]
20. Govender, S.; Friedrich, H. Monoliths: A Review of the Basics, Preparation Methods and Their Relevance to Oxidation. *Catalysts* **2017**, *7*, 62. [CrossRef]
21. Ávila, P.; Montes, M.; Miró, E.E. Monolithic Reactors for Environmental Applications: A Review on Preparation Technologies. *Chem. Eng. J.* **2005**, *109*, 11–36. [CrossRef]
22. Bortolozzi, J.P.; Gutierrez, L.B.; Ulla, M.A. Efficient structured catalysts for ethylene production through the ODE reaction: Ni and Ni-Ce on ceramic foams. *Catal. Commun.* **2014**, *43*, 197–201. [CrossRef]
23. Brussino, P.; Bortolozzi, J.P.; Milt, V.G.; Banús, E.D.; Ulla, M.A. $NiCe/\gamma\text{-}Al_2O_3$ coated onto cordierite monoliths applied to Oxidative Dehydrogenation of Ethane (ODE). *Catal. Today* **2016**, *273*, 259–265. [CrossRef]
24. Brussino, P.; Bortolozzi, J.P.; Milt, V.G.; Banús, E.D.; Ulla, M.A. Alumina-Supported Nickel onto Cordierite Monoliths for Ethane Oxidehydrogenation: Coating Strategies and Their Effect on the Catalytic Behavior. *Ind. Eng. Chem. Res.* **2016**, *55*, 1503–1512. [CrossRef]
25. Donsì, F.; Pirone, R.; Russo, G. Oxidative Dehydrogenation of Ethane over a Perovskite-Based Monolithic Reactor. *J. Catal.* **2002**, *209*, 51–61. [CrossRef]
26. Bortolozzi, J.P.; Banús, E.D.; Terzaghi, D.; Gutierrez, L.B.; Milt, V.G.; Ulla, M.A. Novel catalytic ceramic papers applied to oxidative dehydrogenation of ethane. *Catal. Today* **2013**, *216*, 24–29. [CrossRef]
27. Bortolozzi, J.P.; Banús, E.D.; Courtalón, N.L.; Ulla, M.A.; Milt, V.G.; Miró, E.E. Flexible NiZr-based structured catalysts for ethylene production through ODH of ethane: Catalytic performance enhancement. *Catal. Today* **2016**, *273*, 252–258. [CrossRef]
28. Bortolozzi, J.P.; Banús, E.D.; Milt, V.G.; Miro, E.E. New formulations of Ni-containing ceramic papers to enhance the catalytic performance for the oxidative dehydrogenation of ethane. *Ind. Eng. Chem. Res.* **2014**, *53*, 17570–17579. [CrossRef]
29. Bortolozzi, J.P.; Weiss, T.; Gutierrez, L.B.; Ulla, M.A. Comparison of Ni and $Ni\text{-}Ce/Al_2O_3$ catalysts in granulated and structured forms: Their possible use in the oxidative dehydrogenation of ethane reaction. *Chem. Eng. J.* **2014**, *246*, 343–352. [CrossRef]
30. Santander, J.A.; López, E.; Tonetto, G.M.; Pedernera, M.N. Preparation of NiNbO/AISI 430 Ferritic Stainless Steel Monoliths for Catalytic Applications. *Ind. Eng. Chem. Res.* **2014**, *53*, 11312–11319. [CrossRef]

31. Merino, D.; Sanz, O.; Montes, M. Effect of the thermal conductivity and catalyst layer thickness on the Fischer-Tropsch synthesis selectivity using structured catalysts. *Chem. Eng. J.* **2017**, *327*, 1033–1042. [CrossRef]
32. Sanz, O.; Velasco, I.; Reyero, I.; Legorburu, I.; Arzamendi, G.; Gandía, L.M.; Montes, M. Effect of the thermal conductivity of metallic monoliths on methanolsteam reforming. *Catal. Today* **2016**, *273*, 131–139. [CrossRef]
33. Almeida, L.C.; Echave, F.J.; Sanz, O.; Centeno, M.A.; Odriozola, J.A.; Montes, M. Washcoating of metallic monoliths and microchannel reactors. *Stud. Surf. Sci. Catal.* **2010**, *175*, 25–33. [CrossRef]
34. Palacín, S.; Gutiérrez, A.; Preda, I.; Hernández-Vélez, M.; Sanz, R.; Jiménez, J.A.; Soriano, L. Core-level electronic properties of nanostructured NiO coatings. *Appl. Surf. Sci.* **2007**, *254*, 278–280. [CrossRef]
35. Qin, H.; Guo, C.; Wu, Y.; Zhang, J. Effect of La_2O_3 promoter on NiO/Al_2O_3 catalyst in CO methanation. *Korean J. Chem. Eng.* **2014**, *31*, 1168–1173. [CrossRef]
36. Abdeldayem, H.M.; Faiz, M.; Abdel-Samad, H.S.; Hassan, S.A. Rare earth oxides doped NiO/γ-Al_2O_3 catalyst for oxidative dehydrogenation of cyclohexane. *J. Rare Earths* **2015**, *33*, 611–618. [CrossRef]
37. Sepehri, S.; Rezaei, M.; Garbarino, G.; Busca, G. Preparation and characterization of mesoporous nanocrystalline La-, Ce-, Zr-, Sr-containing Ni-Al_2O_3 methane autothermal reforming catalysts. *Int. J. Hydrogen Energy* **2016**, *41*, 8855–8862. [CrossRef]
38. Mazumder, J.; De Lasa, H.I. Ni catalysts for steam gasification of biomass: Effect of La_2O_3 loading. *Catal. Today* **2014**, *237*, 100–110. [CrossRef]
39. Navarro, R.M.; Guil-Lopez, R.; Ismail, A.A.; Al-Sayari, S.A.; Fierro, J.L.G. Ni- and PtNi-catalysts supported on Al_2O_3 for acetone steam reforming: Effect of the modification of support with Ce, La and Mg. *Catal. Today* **2015**, *242*, 60–70. [CrossRef]
40. Liu, Z.; Zhou, Z.; He, F.; Chen, B.; Zhao, Y.; Xu, Q. Catalytic decomposition of N_2O over NiO-CeO_2 mixed oxide catalyst. *Catal. Today* **2017**, *293–294*, 56–60. [CrossRef]
41. Skoufa, Z.; Xantri, G.; Heracleous, E.; Lemonidou, A.A. A study of Ni-Al-O mixed oxides as catalysts for the oxidative conversion of ethane to ethylene. *Appl. Catal. A Gen.* **2014**, *471*, 107–117. [CrossRef]
42. Heracleous, E.; Lemonidou, A.A. Ni-Nb-O mixed oxides as highly active and selective catalysts for ethene production via ethane oxidative dehydrogenation. Part II: Mechanistic aspects and kinetic modeling. *J. Catal.* **2006**, *237*, 175–189. [CrossRef]
43. Tronconi, E.; Groppi, G.; Visconti, C.G. Structured catalysts for non-adiabatic applications. *Curr. Opin. Chem. Eng.* **2014**, *5*, 55–67. [CrossRef]
44. Sanz, O.; Echave, F.; Romero-Sarria, F.; Odriozola, J.A. Montes, M. Advances in structured and microstructured catalytic reactors for hydrogen production. In *Renewable Hydrogen Technologies: Production, Purification, Storage, Applications and Safety*, 1st ed.; Elsevier: Amsterdam, The Netherlands, 2013; pp. 201–224.

© 2018 by the authors. Licensee MDPI, Basel, Switzerland. This article is an open access article distributed under the terms and conditions of the Creative Commons Attribution (CC BY) license (http://creativecommons.org/licenses/by/4.0/).